LETTER

doi:10.1038/nature17960

Overcoming EGFR(T790M) and EGFR(C797S) resistance with mutant-selective allosteric inhibitors

Yong Jia[1], Cai-Hong Yun[2,3]†, Eunyoung Park[2,3], Dalia Ercan[4], Mari Manuia[1], Jose Juarez[1], Chunxiao Xu[4], Kevin Rhee[4], Ting Chen[4], Haikuo Zhang[4], Sangeetha Palakurthi[5], Jaebong Jang[2,3], Gerald Lelais[1], Michael DiDonato[1], Badry Bursulaya[1], Pierre-Yves Michellys[1], Robert Epple[1], Thomas H. Marsilje[1], Matthew McNeill[1], Wenshuo Lu[1], Jennifer Harris[1], Steven Bender[1], Kwok-Kin Wong[4,5], Pasi A. Jänne[4,5] & Michael J. Eck[2,3]

The epidermal growth factor receptor (EGFR)-directed tyrosine kinase inhibitors (TKIs) gefitinib, erlotinib and afatinib are approved treatments for non-small cell lung cancers harbouring activating mutations in the EGFR kinase[1,2], but resistance arises rapidly, most frequently owing to the secondary T790M mutation within the ATP site of the receptor[3,4]. Recently developed mutant-selective irreversible inhibitors are highly active against the T790M mutant[5,6], but their efficacy can be compromised by acquired mutation of C797, the cysteine residue with which they form a key covalent bond[7]. All current EGFR TKIs target the ATP-site of the kinase, highlighting the need for therapeutic agents with alternative mechanisms of action. Here we describe the rational discovery of EAI045, an allosteric inhibitor that targets selected drug-resistant EGFR mutants but spares the wild-type receptor. The crystal structure shows that the compound binds an allosteric site created by the displacement of the regulatory C-helix in an inactive conformation of the kinase. The compound inhibits L858R/T790M-mutant EGFR with low-nanomolar potency in biochemical assays. However, as a single agent it is not effective in blocking EGFR-driven proliferation in cells owing to differential potency on the two subunits of the dimeric receptor, which interact in an asymmetric manner in the active state[8]. We observe marked synergy of EAI045 with cetuximab, an antibody therapeutic that blocks EGFR dimerization[9,10], rendering the kinase uniformly susceptible to the allosteric agent. EAI045 in combination with cetuximab is effective in mouse models of lung cancer driven by EGFR(L858R/T790M) and by EGFR(L858R/T790M/C797S), a mutant that is resistant to all currently available EGFR TKIs. More generally, our findings illustrate the utility of purposefully targeting allosteric sites to obtain mutant-selective inhibitors.

Diverse activating mutations within the EGFR kinase domain give rise to a subset of non-small cell lung cancers (NSCLCs). The L858R point mutation and small in-frame deletions in the region encoded by exon 19 are the most common mutations, and are among a subset of oncogenic EGFR alterations that confer enhanced sensitivity to EGFR-directed TKIs[11–13]. The dose-limiting toxicity of anilinoquinazoline TKIs such as erlotinib and gefitinib arises from inhibition of wild-type EGFR in the skin and GI tract, thus this enhanced sensitivity relative to wild-type EGFR creates a therapeutic window that allows effective treatment of patients whose tumours are driven by these mutations. The T790M resistance mutation closes this window, in part by increasing the affinity of the mutant receptor for ATP, which in turn diminishes the potency of these ATP-competitive inhibitors[14]. Mutant-selective irreversible inhibitors, including the tool compound WZ4002 (ref. 15) and the clinical compounds osimertinib (AZD9291)[6,16] and rociletinib (CO-1686)[5], are based on a pyrimidine scaffold, and also incorporate a Michael acceptor group that forms a covalent bond with Cys797 at the edge of the ATP binding pocket. Because they bind irreversibly, these agents overcome the enhanced ATP affinity conferred by the T790M mutation. Compounds of this class are demonstrating significant efficacy against T790M mutant tumours in ongoing clinical trials[17,18], and osimertinib was recently approved by the US Food and Drug Administration for patients with *EGFR* T790M-positive NSCLC following progression on previous EGFR TKI therapy. However, laboratory studies and early clinical experience indicate that the efficacy of these agents can be compromised by mutation of Cys797, which thwarts formation of the potency-conferring covalent bond[7,15,19].

Reasoning that an allosteric inhibitor could also overcome the enhanced ATP affinity conferred by the T790M mutation, we screened an ~2.5 million compound library using purified EGFR(L858R/T790M) kinase. The biochemical screen was carried out using 1 μM ATP, and active compounds were counter-screened at 1 mM ATP and against wild-type EGFR to identify those that were potentially non-ATP-competitive and mutant selective. Among the compounds identified in the screen, EGFR allosteric inhibitor-1 (EAI001, Fig. 1a) was of particular interest owing to its potency and selectivity for mutant EGFR (half maximal inhibitory concentration (IC_{50}) = 0.024 μM for L858R/T790M at 1 mM ATP, IC_{50} > 50 μM for wild-type EGFR). Further characterization of the mutant-selectivity of EAI001 revealed modest potency against the isolated L858R and T790M mutants (0.75 μM and 1.7 μM, respectively, Extended Data Fig. 1a). Medicinal-chemistry-based optimization of this compound yielded EAI045 (Fig. 1a), a 3 nM inhibitor of the L858R/T790M mutant with ~1000-fold selectivity versus wild-type EGFR at 1 mM ATP (Table 1). Enzyme kinetic characterization confirmed that the mechanism of inhibition was not competitive with respect to ATP (Table 1, Extended Data Fig. 1b). Profiling of EAI045 against a panel of 250 protein kinases revealed pronounced selectivity; no other kinases were inhibited by more than 20% at 1 μM EAI045 (Extended Data Table 1). Evaluation of EAI045 in a safety pharmacology assay panel revealed also excellent selectivity against non-kinase targets (Extended Data Table 2).

The crystal structure of EAI001 bound to T790M-mutant EGFR showed that the compound binds in an allosteric pocket that is created in part by the outward displacement of the C-helix in the inactive conformation of the kinase (Fig. 1b, c, Extended Data Table 3). The compound binds as a 'three-bladed propeller' with the aminothiazole moiety inserted between the mutant gatekeeper methionine and active site residue Lys745. The phenyl substituent extends into a hydrophobic cleft at the back of the pocket and is in contact with Leu777 and Phe856. Finally, the 1-oxoisoindolinyl group extends along the C-helix towards the solvent exposed exterior. The compound also forms a hydrogen bond with Asp855 in the DFG motif. In further support of

[1]Genomics Institute of the Novartis Research Foundation, San Diego, California 92121, USA. [2]Department of Cancer Biology, Dana-Farber Cancer Institute, Boston, Massachusetts 02215, USA. [3]Department of Biological Chemistry and Molecular Pharmacology, Harvard Medical School, Boston, Massachusetts 02115, USA. [4]Lowe Center for Thoracic Oncology, Dana-Farber Cancer Institute, Boston, Massachusetts 02215, USA. [5]Belfer Center for Applied Cancer Science, Dana-Farber Cancer Institute, Boston, Massachusetts 02215, USA. †Present address: Peking University Institute of Systems Biomedicine and Department of Biophysics, Peking University Health Science Center, Beijing 100191, China.

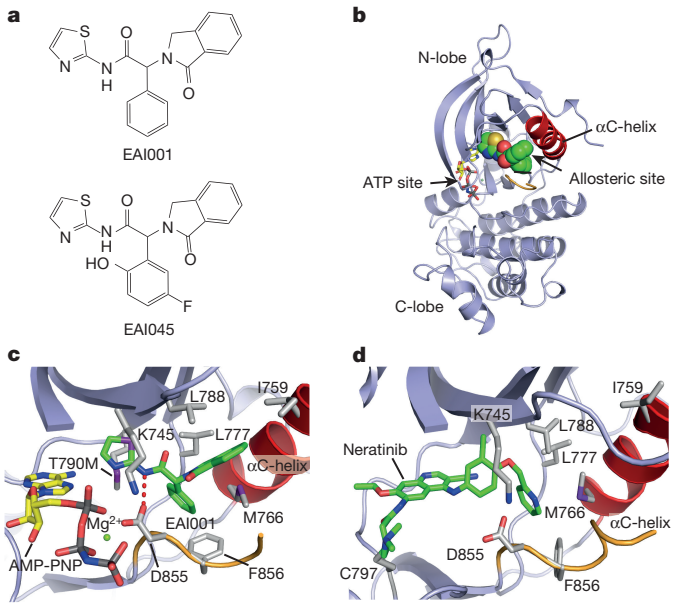

Figure 1 | Structure and binding mode of allosteric EGFR inhibitors. **a**, Chemical structures of EAI001 and EAI045. **b**, Overall view of the structure of EGFR(T790M/V948R) bound to EAI001 and AMP-PNP. EAI001 is shown in CPK-coloured form with carbon atoms in green. The V948R substitution was introduced to allow crystallization of the kinase in an inactive conformation[8]. **c**, Detailed view of the interactions of EAI001. A hydrogen bond with Asp855 in the DFG-motif of the kinase activation loop is shown as a dashed red line. **d**, The structure of irreversible inhibitor neratinib bound to EGFR(T790M) (PDB, 2JIV). Neratinib occupies the ATP site, but also extends into the allosteric pocket occupied by EAI001.

a non-ATP competitive mechanism, the ATP-analogue adenylyl-imidodiphosphate (AMP-PNP) is bound in the expected manner in the active site cleft (Fig. 1c).

Interestingly, the EGFR inhibitors neratinib[20] and lapatinib[21] extend into the allosteric site and make interactions that resemble those of two of the three blades of the allosteric agents (Fig. 1d, Extended Data Fig. 2a, c). These ATP-competitive inhibitors are not mutant selective, and they span both the ATP and allosteric sites. Additionally, we note that the EGFR allosteric pocket is roughly analogous to a site in MEK1 that is targeted by a number of allosteric inhibitors that are now approved or in clinical trials[22]. Despite the similar location of the MEK allosteric site, there is no structural correspondence in the binding modes of the respective allosteric inhibitors (Extended Data Fig. 2a, b).

The mutant-specificity of the EGFR allosteric inhibitors arises from at least two effects. Most apparently, the direct contact of the aminothiazole group with the mutant gatekeeper methionine residue can explain the selectivity for the T790M mutant. Second, the compound cannot bind the fully inactive conformation of the wild-type kinase; simple modelling reveals steric clashes of EAI001 with Leu858 and Leu861 in the N-terminal portion of the activation loop (Extended Data Fig. 3). The L858R mutation rearranges this portion of the activation loop[23], thereby enlarging the allosteric pocket. EAI045 may also inhibit other mutants with a similar mechanism of activation, such as L861Q, but we do not expect it to inhibit most exon 19 deletion variants. These mutations shorten the loop leading into the C-helix and may therefore prevent opening of the allosteric pocket.

Initial studies of the cellular activity of EAI045 showed that it potently decreased, but did not completely eliminate, EGFR autophosphorylation in H1975 cells, an L858R/T790M-mutant NSCLC cell line (Fig. 2a). A similar effect was observed in NIH-3T3 cells stably transfected with the L858R/T790M mutant (Extended Data Fig. 4a). This inhibition was selective for mutant EGFR; EAI045 potently inhibited EGFR Y1173 phosphorylation in H1975 cells (half maximal effective concentration (EC_{50}) = 2 nM), but not in HaCaT cells, a keratinocyte

Table 1 | Inhibitory activity of EAI045 on wild type EGFR and selected mutants

ATP (μM)	EAI045 IC_{50} (μM)			
	Wild type	L858R	T790M	L858R/T790M
1	1.6	0.076	0.049	0.002
10	1.9	0.019	0.19	0.002
100	3.5	0.009	0.5	0.003
1000	4.3	0.009	0.6	0.003

cell line with wild-type EGFR (Extended Data Table 4). We observed an intermediate level of activity in the L858R-mutant H3255 cells, a pattern consistent with our biochemical inhibition data (Extended Data Table 4). Despite potent inhibition of mutant EGFR, EAI045 showed no anti-proliferative effect in the H1975 and H3255 cell lines with concentrations as high as 10 μM (Extended Data Table 4). Profiling in a panel of EGFR-mutant Ba/F3 cells revealed that EAI045 inhibited proliferation of L858R/T790M and L858R mutant cells, but not the exon19del/T790M or parental Ba/F3 cells, indicative of on-target mutant-selective activity of the allosteric inhibitor (Extended Data Fig. 4b–e). However, half-maximal inhibition required ~10 μM EAI045, a concentration much higher than the biochemical IC_{50} of the compound.

In light of the incomplete inhibition of EGFR autophosphorylation and the allosteric mechanism of action of EAI045, we wondered to what extent ligand stimulation would affect inhibition of the mutant receptor. We compared inhibition of EGFR Y1173 phosphorylation in H1975 cells in the presence and absence of exogenous EGF (10 ng ml^{-1}) using an ELISA-based assay. EAI045 inhibited EGFR phosphorylation with a similar EC_{50} irrespective of EGF stimulation, but notably, inhibition plateaued at 50% in the presence of ligand (Fig. 2b). This phenomenon suggests two populations of receptor, one that remains sensitive to the allosteric inhibitor upon ligand stimulation, and another, equal in number, that is rendered insensitive. Ligand-induced dimerization of the EGF receptor is known to induce an asymmetric interaction of the kinase domains[8], and is an apparent potential source of two receptor populations with differential inhibitor sensitivity.

In the EGFR asymmetric dimer, the C-lobe of the 'activator' subunit impinges on the N-lobe of the 'receiver' subunit, inducing an active conformation in the receiver by reorienting the regulatory C-helix to its inward position (Fig. 2c). In wild-type EGFR, only the receiver subunit is activated. By contrast, both subunits in a mutant receptor are expected to be catalytically active, because oncogenic kinase domain mutations induce the active conformation even in the absence of ligand. As explained above, EAI045 binds a 'C-helix out' conformation of the kinase. In the receiver subunit but not the activator, outward displacement of the C-helix is impeded by the asymmetric dimer interaction. Therefore, we hypothesized that EAI045 was a potent inhibitor of the activator subunit of the mutant receptor, but a much less potent inhibitor of the receiver subunit, in which the C-helix is captive. Because the mutant receptor favours dimer formation[24,25], this effect could explain both the incomplete inhibition of EGFR autophosphorylation and the apparent disconnect in the biochemical and cellular potencies of the allosteric inhibitor. To test this notion, we exploited an I941R point mutation in the C-lobe of the kinase, which is known to block the asymmetric dimer interaction[8,26]. The activity of the L858R/T790M mutant is dimerization-independent[26] and, as expected, transduction of Ba/F3 cells with EGFR(L858R/T790M/I941R) led to factor-independent proliferation. In support of our hypothesis, Ba/F3 cells bearing this dimerization-defective mutant were markedly more sensitive to the allosteric inhibitor (Fig. 2d).

The therapeutic antibody cetuximab targets the extracellular portion of the EGF receptor, blocking ligand binding and preventing dimer formation[9,10]. The antibody is not effective clinically in EGFR-mutant NSCLC, and in cell-based studies cetuximab alone does not inhibit L858R/T790M or exon19del/T790M mutant EGFR, because their activity is independent of dimerization[26]. However, we reasoned that

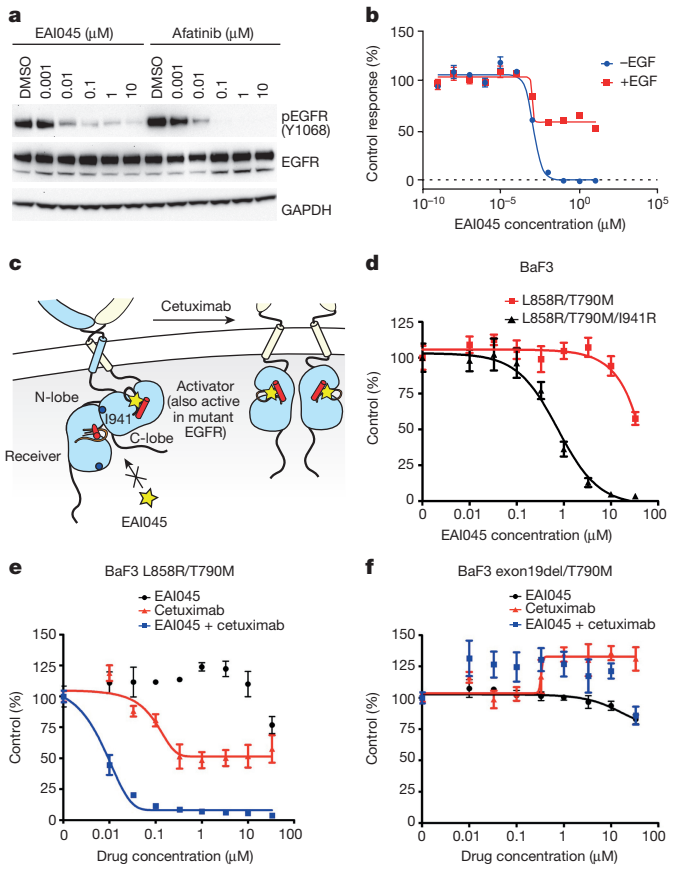

Figure 2 | Cellular activity and mechanism of synergy of EAI045 with cetuximab. a, Analysis of EAI045 inhibition of EGFR phosphorylation in H1975 cells by western blotting (anti-pY1068). A dose response study is shown at 3 h after compound addition for EAI045 and the irreversible quinazoline inhibitor afatinib (control). For gel source data, see Supplementary Fig. 1. **b**, The effect of EAI045 on EGFR target modulation in H1975 cells in the presence and absence of EGF. EGFR phosphorylation (pY1173) was measured using an ELISA-based assay; error bars indicate s.d. ($n = 3$). **c**, The allosteric pocket is differentially accessible in the two subunits of the asymmetric dimer. Unlike wild-type EGFR in which only the receiver subunit is active, both subunits are catalytically active in the L858R/T790M mutant. The activator subunit is more readily inhibited by allosteric agents (yellow star), because the C-helix can be readily displaced. By contrast, opening the allosteric pocket in the receiver subunit requires perturbing the dimer. Thus mutations that disrupt the asymmetric dimer (such as I941R, blue circle) or antibodies that block dimerization (cetuximab) should enhance the potency of allosteric agents. **d**, Inhibition of proliferation of Ba/F3 cells expressing L858R/T790M and L858R/T790M/I941R by EAI045. Addition of the dimer-disrupting I941R mutation markedly increased inhibition by EAI045. **e**, **f**, Treatment of EGFR-mutant Ba/F3 cells with EAI045 alone, in combination with cetuximab (10 μg ml^{-1}), or with cetuximab alone. Note the pronounced synergy with cetuximab that is observed only in the L858R/T790M model. The mean ± s.d. ($n = 6$) is plotted for each drug and concentration (**d**–**f**).

cetuximab should synergize with a kinase-targeted allosteric inhibitor, by converting the inhibitor-resistant receiver population into a monomeric form that is remarkably sensitive to EAI045. Notably, in the presence of cetuximab (10 μg ml^{-1}), EAI045 inhibited proliferation of EGFR(L858R/T790M) Ba/F3 cells with an IC_{50} of approximately 10 nM, similar to its potency against this mutant in biochemical assays (Fig. 2e). In support of an on-target, mutant-selective effect of the allosteric agent, proliferation of Ba/F3 cells bearing EGFR(exon19del/T790M) was not inhibited by this combination (Fig. 2f).

We next tested the *in vivo* efficacy of EAI045 in genetically engineered mouse model of L858R/T790M-mutant-driven lung cancer[27], both alone and in combination with cetuximab. Mouse

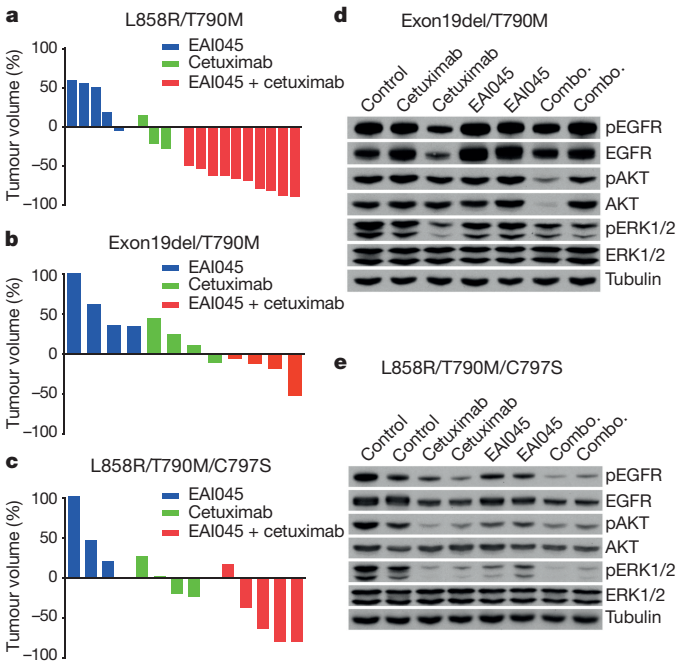

Figure 3 | EAI045 in combination with cetuximab induces tumour regression in genetically engineered mouse models of EGFR-mutant lung cancer. a, Mice bearing L858R/T790M mutant tumours were treated with EAI045 alone ($n = 5$), cetuximab alone ($n = 3$) or both agents in combination ($n = 10$). Tumour volumes were measured using MRI 4 weeks after initiation of treatment and are plotted for each animal in a 'waterfall' format. **b**, As in **a**, but in mice bearing exon19del/T790M mutant tumours ($n = 4$, 4 and 4). **c**, As in **a**, but in mice bearing L858R/T790M/C797S mutant tumours ($n = 3$, 4, and 5). **d**, **e**, Pharmacodynamic studies in exon19del/T790M and L858R/T790M/C797S mice. Tumour nodules from mice treated with EAI045 or cetuximab alone or with the combination (combo.) were analysed by western blotting with the indicated antibodies to examine the effect of treatment on EGFR signalling. Multiple independent mouse tumours were obtained and analysed, two independent and representative samples are shown. For gel source data, see Supplementary Fig. 1. Source data for tumour volume measurements are provided in Supplementary Fig. 2.

pharmacokinetic studies with EAI045 revealed a maximal plasma concentration of 0.57 μM, a half-life of 2.15 h, and oral bioavailability of 26% after dosing at 20 mg kg^{-1}. In a 4-week efficacy study, mice were treated with EAI045 at 60 mg kg^{-1} by oral gavage once daily, either alone or together with cetuximab (1 mg intraperitoneally every other day). We observed marked tumour regressions in the L858R/T790M-mutant mice treated with the combination, whereas those treated with EAI045 alone did not respond (Fig. 3a). Cetuximab alone had a very modest effect in these mice, as previously observed[26]. Mice bearing EGFR(exon19del/T790M) were treated using the same protocol, but as expected failed to respond to the combination therapy (Fig. 3b). Magnetic resonance imaging (MRI) studies of cohorts of L858R/T790M and exon19del/T790M mice after combination treatment for 1 or 2 weeks are shown in Extended Data Fig. 5.

Mutation of C797 is expected to confer resistance to all third-generation irreversible EGFR inhibitors that are active on the T790M-mutant EGFR, and a preliminary study reported the C797S alteration in 15 out of 67 patients (22%) with acquired resistance to AZD9291 (ref. 28). Mutations in C797 should not affect the efficacy of EAI045, as this residue is remote from the allosteric binding pocket. Consistent with this expectation, EAI045 in combination with cetuximab potently inhibited L858R/T790M/C797S Ba/F3 cells (Extended Data Fig. 5a) and treatment of genetically engineered L858R/T790M/C797S mice with EAI045 and cetuximab induced marked tumour shrinkage, similar to that observed in the L858R/T790M models (Fig. 3c, Extended Data Fig. 5b). Pharmacodynamic studies performed following two doses

of treatment demonstrated that EAI045 in combination with cetuximab effectively inhibited phosphorylation of EGFR and downstream signalling proteins in these mice, but not in mice bearing the insensitive exon19del/T790M mutation (Fig. 3d, e).

The compounds we describe here are among the first allosteric TKIs, and to our knowledge, the first targeting any receptor tyrosine kinase in a mutant-selective manner. Further study is required, but our findings suggest that EAI045 or a related compound in combination with an EGFR dimer-disrupting antibody such as cetuximab would be an effective strategy for treating L858R/T790M-mutant-driven lung cancers, as well as those driven by the triple L858R/T790M/C797S mutation, which are resistant to all current EGFR-targeted therapies. EAI045 and cetuximab exhibit mechanistic synergy, a valuable property for combination agents because it lowers the dose required for efficacy. Ideally, chemotherapeutic agents used in combination should also have non-overlapping mechanisms of toxicity and sensitivity to resistance mutations. EAI045 meets these criteria as well; its lack of activity on wild-type EGFR and other kinases suggest that its dose-limiting toxicity is unlikely to be related to that of cetuximab and ATP-competitive EGFR inhibitors. In addition, given its distinct binding site, its sensitivity to resistance-conferring mutations is expected to be divergent from that of both cetuximab and ATP-site inhibitors. For these reasons, we speculate that an allosteric agent like EAI045 could be used in combination with ATP-site-directed inhibitors, with the goal of preventing the emergence of treatment-associated resistance mutations in the receptor itself.

Online Content Methods, along with any additional Extended Data display items and Source Data, are available in the online version of the paper; references unique to these sections appear only in the online paper.

Received 15 October 2015; accepted 29 March 2016.
Published online 25 May 2016.

1. Mok, T. S. *et al.* Gefitinib or carboplatin-paclitaxel in pulmonary adenocarcinoma. *N. Engl. J. Med.* **361,** 947–957 (2009).
2. Yu, H. A. & Pao, W. Targeted therapies: Afatinib—new therapy option for EGFR-mutant lung cancer. *Nat. Rev. Clin. Oncol.* **10,** 551–552 (2013).
3. Gainor, J. F. & Shaw, A. T. Emerging paradigms in the development of resistance to tyrosine kinase inhibitors in lung cancer. *J. Clin. Oncol.* **31,** 3987–3996 (2013).
4. Chong, C. R. & Jänne, P. A. The quest to overcome resistance to EGFR-targeted therapies in cancer. *Nat. Med.* **19,** 1389–1400 (2013).
5. Walter, A. O. *et al.* Discovery of a mutant-selective covalent inhibitor of EGFR that overcomes T790M-mediated resistance in NSCLC. *Cancer Discov.* **3,** 1404–1415 (2013).
6. Finlay, M. R. *et al.* Discovery of a potent and selective EGFR inhibitor (AZD9291) of both sensitizing and T790M resistance mutations that spares the wild type form of the receptor. *J. Med. Chem.* **57,** 8249–8267 (2014).
7. Thress, K. S. *et al.* Acquired *EGFR C797S* mutation mediates resistance to AZD9291 in non-small cell lung cancer harboring *EGFR* T790M. *Nat. Med.* **21,** 560–562 (2015).
8. Zhang, X., Gureasko, J., Shen, K., Cole, P. A. & Kuriyan, J. An allosteric mechanism for activation of the kinase domain of epidermal growth factor receptor. *Cell* **125,** 1137–1149 (2006).
9. Goldstein, N. I., Prewett, M., Zuklys, K., Rockwell, P. & Mendelsohn, J. Biological efficacy of a chimeric antibody to the epidermal growth factor receptor in a human tumor xenograft model. *Clin. Cancer Res.* **1,** 1311–1318 (1995).
10. Li, S. *et al.* Structural basis for inhibition of the epidermal growth factor receptor by cetuximab. *Cancer Cell* **7,** 301–311 (2005).
11. Paez, J. G. *et al. EGFR* mutations in lung cancer: correlation with clinical response to gefitinib therapy. *Science* **304,** 1497–1500 (2004).
12. Pao, W. *et al.* EGF receptor gene mutations are common in lung cancers from "never smokers" and are associated with sensitivity of tumors to gefitinib and erlotinib. *Proc. Natl Acad. Sci. USA* **101,** 13306–13311 (2004).
13. Lynch, T. J. *et al.* Activating mutations in the epidermal growth factor receptor underlying responsiveness of non-small-cell lung cancer to gefitinib. *N. Engl. J. Med.* **350,** 2129–2139 (2004).
14. Yun, C. H. *et al.* The T790M mutation in EGFR kinase causes drug resistance by increasing the affinity for ATP. *Proc. Natl Acad. Sci. USA* **105,** 2070–2075 (2008).
15. Zhou, W. *et al.* Novel mutant-selective EGFR kinase inhibitors against EGFR T790M. *Nature* **462,** 1070–1074 (2009).
16. Cross, D. A. *et al.* AZD9291, an irreversible EGFR TKI, overcomes T790M-mediated resistance to EGFR inhibitors in lung cancer. *Cancer Discov.* **4,** 1046–1061 (2014).
17. Sequist, L. V. *et al.* Rociletinib in *EGFR*-mutated non-small-cell lung cancer. *N. Engl. J. Med.* **372,** 1700–1709 (2015).
18. Jänne, P. A. *et al.* AZD9291 in EGFR inhibitor-resistant non-small-cell lung cancer. *N. Engl. J. Med.* **372,** 1689–1699 (2015).
19. Ercan, D. *et al.* EGFR mutations and resistance to irreversible pyrimidine-based EGFR inhibitors. *Clin. Cancer Res.* **21,** 3913–3923 (2015).
20. Tsou, H. R. *et al.* Optimization of 6,7-disubstituted-4-(arylamino)quinoline-3-carbonitriles as orally active, irreversible inhibitors of human epidermal growth factor receptor-2 kinase activity. *J. Med. Chem.* **48,** 1107–1131 (2005).
21. Wood, E. R. *et al.* A unique structure for epidermal growth factor receptor bound to GW572016 (Lapatinib): relationships among protein conformation, inhibitor off-rate, and receptor activity in tumor cells. *Cancer Res.* **64,** 6652–6659 (2004).
22. Zhao, Y. & Adjei, A. A. The clinical development of MEK inhibitors. *Nat. Rev. Clin. Oncol.* **11,** 385–400 (2014).
23. Yun, C. H. *et al.* Structures of lung cancer-derived EGFR mutants and inhibitor complexes: mechanism of activation and insights into differential inhibitor sensitivity. *Cancer Cell* **11,** 217–227 (2007).
24. Red Brewer, M. *et al.* Mechanism for activation of mutated epidermal growth factor receptors in lung cancer. *Proc. Natl Acad. Sci. USA* **110,** E3595–E3604 (2013).
25. Shan, Y. *et al.* Oncogenic mutations counteract intrinsic disorder in the EGFR kinase and promote receptor dimerization. *Cell* **149,** 860–870 (2012).
26. Cho, J. *et al.* Cetuximab response of lung cancer-derived EGF receptor mutants is associated with asymmetric dimerization. *Cancer Res.* **73,** 6770–6779 (2013).
27. Li, D. *et al.* Bronchial and peripheral murine lung carcinomas induced by T790M-L858R mutant EGFR respond to HKI-272 and rapamycin combination therapy. *Cancer Cell* **12,** 81–93 (2007).
28. Oxnard, G. R. *et al.* in *16th World Conference on Lung Cancer* (Denver, Colorado, 2015).

Supplementary Information is available in the online version of the paper.

Acknowledgements This work was supported in part by NIH grants CA116020 (M.J.E.), CA154303 (M.J.E., K.-K.W. and P.A.J.), CA120964 (K.-K.W.) and CA135257 (P.A.J.), and by the Gross-Loh Family Fund for Lung Cancer Research (K.-K.W.). We thank N. Gray for helpful comments on the manuscript.

Author Contributions M.J.E., P.A.J., K.-K.W., Y.J., G.L., P.-Y.M., J.H., and S.B. coordinated the study. Y.J., M.M., J. Juarez, M.D., B.B., E.P., C.-H.Y., D.E., C.X., K.R., T.C., H.Z., S.P., and J. Jang designed and performed experiments. Y.J., M.M., J. Juarez, M.D., B.B., S.B., E.P., C.-H.Y., D.E., C.X., K.R., M.J.E., P.J., and K.-K.W. interpreted data. M.M., J. Juarez, M.D., G.L., P.-Y.M., R.E., T.H.M, M.M., C-H.Y. and W.L. prepared reagents. Y.J., K.-K.W., P.A.J. and M.J.E. wrote and edited the manuscript.

Author Information The crystal structure of EGFR(T790M/V948R) in complex with EAI001 has been deposited in the Protein Data Bank under accession number 5D41. Reprints and permissions information is available at www.nature.com/reprints. The authors declare competing financial interests: details are available in the online version of the paper. Readers are welcome to comment on the online version of the paper. Correspondence and requests for materials should be addressed to M.J.E. (eck@crystal.harvard.edu).

METHODS

EGFR protein expression and purification. Constructs spanning residues 696–1022 of the human EGFR (including wild type, L858R, L858R/T790M, T790M, and T790M/V948R mutant sequences) were prepared in a GST-fusion format using the pTriEX system (Novagen) for expression in Sf9 insect cells essentially as described[14,23]. EGFR kinase proteins were purified by glutathione-affinity chromatography followed by size-exclusion chromatography after cleavage with Tomato etch virus (TEV) or thrombin to remove the GST fusion partner following established procedures[14,23].

High-throughput screening. Purified EGFR(L858R/T790M) enzyme was screened against Novartis compound collection of ~2.5 million using homogeneous time-resolved fluorescence (HTRF)-based biochemical assay format. The screening was performed at 1 μM ATP using a single compound concentration (12.5 μM). 1,322 top hits were picked for follow-up IC_{50} confirmation. IC_{50} values were determined at both 1 μM and 1 mM ATP to identify both ATP competitive and non-competitive compounds. Hits were also counter-screened against wild-type EGFR to evaluate the mutant selectivity.

HTRF-based EGFR biochemical assays. Biochemical assays for wild-type EGFR and each mutant were carried out using a HTRF assay as described previously[29]. Assays were optimized for each ATP concentration. Compound IC_{50} values were determined by 12-point inhibition curves (from 50 to 0.000282 μM) in duplicate.

Structure determination. Before crystallization, 0.1 mM of EGFR(T790M/V948R) was incubated for 1 h with 0.5 mM EAI001, 1 mM adenosine 5′-(β,γ-imido) triphosphate (AMP-PNP) and 10 mM $MgCl_2$ at room temperature. Crystals of EGFR(T790M/V948R) in complex with EAI001 were prepared by hanging-drop vapour diffusion method over a reservoir solution containing 0.1 M Bis-Tris (pH 5.5), 25% PEG 3350, 5 mM tris (2-carboxyethyl)-phosphine (TCEP). Crystals were flash-frozen in liquid nitrogen after rapid immersion in a cryoprotectant solution containing 0.1M Bis-Tris 5.5, 25% PEG3350, 10% ethylene glycol and 5 mM TCEP. Diffraction data were recorded using a Mar343 image plate detector on a rotating anode source at 100 K. Data were processed and merged as described previously[14]. The structure was determined by molecular replacement with the program PHASER using an inactive EGFR kinase structure (PDB, 2GS7) as the search model. Repeated rounds of manual refitting and crystallographic refinement were performed using COOT and REFMAC. The inhibitor was modelled into the closely fitting positive $F_o - F_c$ electron density and then included in following refinement cycles. Although the EAI001 preparation used in crystallization was racemic, the density clearly corresponded to the *R* stereoisomer and was modelled accordingly. Topology and parameter files for the inhibitors were generated using PRODRG. Statistics for diffraction data processing and structure refinement are shown in Extended Data Table 3.

Tissue Culture. Cells were maintained in 10% FBS/RPMI supplemented with 100 μg ml^{-1} penicillin/streptomycin (Hyclone SH30236.01). The cells were collected with 0.25% trypsin/EDTA (Hyclone SH30042.1), re-suspended in 5% FBS/RPMI penicillin/streptomycin and plated at 7,500 cells per well in 50 μl of media in a 384-well black plate with clear bottoms (Greiner 789068G). The cells were allowed to incubate overnight in a 37 °C, 5% CO_2 humidified tissue culture incubator. The 12-point serial diluted test compounds were transferred to the plate containing cells by using a 50 nl Pin Head device (Perkin Elmer) and the cells were placed back in the incubator for 3 h. All cell lines were tested and found negative for mycoplasma contamination using the MycoAlert Mycoplasma Detection Kit (Lonza).

Phospho-EGFR (Y1173) target modulation assay. HaCaT cells were stimulated with 10 ng ml^{-1} EGF (Peprotech AF-100-15) for 5 min at room temperature. Constitutively activated EGFR mutant cell lines (H1975 and H3255) were not stimulated with EGF. The media was reduced to 20 μl using a Bio-Tek ELx405 Select plate washer. Cells were lysed with 20 μL of 2× lysis buffer containing protease and phosphatase inhibitors (2% Triton X-100, 40 mM Tris (pH 7.5), 2 mM EDTA, 2 mM EGTA, 300 mM NaCl, 2× complete cocktail inhibitor (Roche 11 697 498 001), 2× phosphatase inhibitor cocktail set II and set III (Sigma P5726 and P0044)). The plates were shaken for 20 min. An aliquot of 25 μl from each well was transferred to prepared ELISA plates for analysis.

For the experiment studying the effect of EGF pre-treatment on EAI045 target modulation, H1975 cells were collected and plated in 0.5% FBS/RPMI penicillin/streptomycin. On the following day, cells were pre-treated with 0.5% FBS/RPMI media with or without 10 ng EGF per ml for 5 min. Compound was added and assay was carried out as described above. The experiment was performed twice with duplicate samples in each experiment.

Phospho-EGFR (Y1173) ELISA. Solid white 384-well high-binding ELISA plates (Greiner 781074) were coated with 5 μg ml^{-1} goat anti-EGFR capture antibody overnight in 50 mM carbonate/bicarbonate (pH 9.5) buffer. Plates were blocked with 1% BSA (Sigma A7030) in PBS for 1 h at room temperature, and washes were carried out with a Bio-Tek ELx405 Select using four cycles of 100 μl TBS-Tween (20 mM Tris, 137 mM NaCl, 0.05% Tween-20) per well. A 25 μl aliquot of lysed cell was added to each well of the ELISA plate and incubated overnight at 4 °C with gentle shaking. After washing, 1:1,000 anti-phospho-EGFR in 0.2% BSA/TBS-Tween was added and incubated for 2 h at room temperature. After washing, 1:2,000 anti-rabbit-HRP (horseradish peroxidase) in 0.2% BSA/TBS-Tween was added and incubated for 1 h at room temperature. Chemiluminescent detection was carried out with SuperSignal ELISA Pico substrate. Luminescence was read with an EnVision plate reader.

Western blotting. Cell lysates were equalized to protein content determined by Coomassie Plus protein assay reagent (ThermoScientific 1856210) and loaded onto 4–12% NuPAGE Bis-Tris gels with MOPS running buffer with LDS Sample buffer supplemented with DTT. Gel proteins were transferred to PVDF membranes with an iBlot Gel Transfer Device. 1× Casein-blocked membranes were probed with primary antibodies overnight at 4 °C on an end-over-end rotisserie. Membranes were washed with TBS-Tween and HRP-conjugated secondary antibodies were added for 1 h at room temperature. After washing, HRP was detected using Luminata Forte Western HRP Substrate reagent and recorded with a Bio-Rad VersaDoc imager.

H1975, H3255 and HaCaT proliferation assays. H1975, H3255 and HaCaT cell lines were plated in solid white 384-well plates (Greiner) at 500 cells per well in 10% FBS RPMI penicillin/streptomycin media. Using a Pin Tool, 50 nl of serial diluted compounds were transferred to the cells. After 3 days, cell viability was measured by CellTiter-Glo (Promega) according to manufacturer's instructions. Luminescent readout was normalized to 0.1% DMSO-treated cells and empty wells. Data was analysed by nonlinear regression curve fitting and EC_{50} values were reported.

Ba/F3 cell proliferation models. The EGFR mutant L858R, L858R/T790M, delE746_A750/T790M, L858R/T790M/C797S and del/T790M/C797S Ba/F3 cells have been previously described[15]. The EGFR(I941R) mutation was introduced via site directed mutagenesis using the Quick Change Site-Directed Mutagenesis kit (Stratagene) according to the manufacturer's instructions. All constructs were confirmed by DNA sequencing. The constructs were shuttled into the retroviral vector JP1540 using the BD Creator System (BD Biosciences). Ba/F3 cells were infected with retrovirus and according to standard protocols, as described previously[30]. Stable clones were obtained by selection in puromycin (2 μg ml^{-1}). Ba/F3 cells have not been authenticated as there is no publicly available fingerprint for Ba/F3 cells. All variants used were confirmed to contain the correct EGFR mutation by sequencing. All Ba/F3 cells were tested for mycoplasma contamination and confirmed to be free of contamination.

Growth and inhibition of growth was assessed by MTS assay and was performed according to previously established methods[15]. Ba/F3 cells of different *EGFR* genotypes were exposed to treatment for 72 h and the number of cells used per experiment determined empirically and has been previously established[15]. All experimental points were set up in six wells and all experiments were repeated at least three times. The data was graphically displayed using GraphPad Prism version 5.0 for Windows, (GraphPad software; http://www.graphpad.com). The curves were fitted using a nonlinear regression model with a sigmoidal dose response.

NIH-3T3 cell studies. NIH-3T3 cells were infected with retroviral constructs expressing *EGFR* mutants according to standard protocols, as described previously[15,19]. Stable clones were obtained by selection in puromycin (2 μg ml^{-1}).

Mouse efficacy studies. EGFR(TL) (bearing L858R/T790M point mutations) and EGFR(TD) (bearing exon19del/T790M point mutations) mice were generated as previously described[15,27]. The EGFR(L858R/T790M/C797S) (denoted as TLCS hereafter) mutant mouse cohort was established briefly as follows: the full-length human TLCS cDNA was generated by site-directed mutagenesis using the Quickchange site directed mutagenesis kit (Agilent Technologies) and further verified by DNA sequencing. Sequence-verified targeting vectors were co-electroporated with an FLPe recombinase plasmid into v6.5 C57BL/6J (female) × 129/sv (male) embryonic stem cells (Open Biosystems) as described elsewhere[31]. Resulting hygromycin-resistant embryonic stem clones were evaluated for transgene integration via PCR. Then, transgene-positive embryonic stem clones were injected into C57BL/6 blastocysts, and the resulting chimaeras were mated with BALB/c wild type mice to determine germline transmission of the TLCS transgene. Further detail on the generation and characterization of the TLCS transgenic mice is provided in Supplementary Fig. 3. Progeny of TL, TD and TLCS mice were genotyped by PCR of tail DNA. The TL and TD mice were fed a doxycycline diet at 6 weeks of age to induce EGFR(TL) or EGFR(TD) expression, respectively. The TLCS mice were intranasally instilled with Ad-Cre (University of Iowa viral vector core) at 6 weeks of age to excise the loxP sites, activating EGFR(TLCS) expression.

The EAI045 compound was dissolved in 10% NMP (10% 1-methyl-2-pyrrolidinone: 90% PEG-300), and was dosed at 60 mg kg^{-1} daily by oral gavage. Cetuximab was administrated at 1 mg $mouse^{-1}$ every other day by intraperitoneal injection. The TL, TD and TLCS mice were monitored by MRI to quantify lung tumour

burden before being assigned to various study treatment cohorts, which were non-blinded and not formally randomized. All treated mice had an equal initial tumour burden. MRI evaluation was repeated every 2 weeks during treatment. The animals were imaged with a rapid acquisition with relaxation enhancement sequence (repetition time = 2000 ms; echo time = 25 ms) in the coronal and axial planes with a 1-mm slice thickness and with respiratory gating. The detailed procedure for MRI scanning has been previously described[27]. The tumour burden volumes were quantified using 3-dimensional Slicer software. Source data for tumour volume measurements are provided in Supplementary Fig. 2.

All care of experimental animals was in accordance with Harvard Medical School/Dana-Farber Cancer Institute institutional animal care and use committee (IACUC) guidelines. All mice were housed in a pathogen-free environment at a DFCI animal facility and handled in strict accordance with Good Animal Practice as defined by the Office of Laboratory Animal Welfare. None of the tumour efficacy experiments presented in this manuscript exceeded the 2 cm maximal diameter tumour size, as permitted by the Dana-Farber Cancer Institute IACUC.

Synthesis and characterization of EAI045. 2-(5-fluoro-2-hydroxyphenyl)-2-(1-oxo-2,3-dihydro-1H-isoindol-2-yl)-*N*-(1,3-thiazol-2-yl)acetamide (EAI045) was prepared from 2-amino-2-(5-fluoro-2-methoxyphenyl)acetic acid using a reaction sequence similar to that previously described[32] followed by demethylation with boron tribromide.

^{1}H NMR (400 MHz, DMSO-d6) δ 12.61 (s, 1H), 9.96 (s, 1H), 7.73 (d, J = 7.5 Hz, 1H), 7.66–7.54 (m, 2H), 7.52 (dd, J = 1.0, 7.4 Hz, 1H), 7.49 (d, J = 3.6 Hz, 1H), 7.27 (d, J = 3.5 Hz, 1H), 7.11 (td, J = 3.2, 8.6 Hz, 1H), 6.90 (dd, J = 4.8, 8.9 Hz, 1H), 6.85 (dd, J = 3.1, 9.2 Hz, 1H), 6.31 (s, 1H), 4.61 (d, J = 17.5 Hz, 1H), 3.98 (d, J = 17.5 Hz, 1H); ^{19}F NMR (376 MHz, DMSO-d6) δ −125.15 (s, 1F); LCMS: Rt 1.278 min; ESMS m/z 384.20 ($M^{+}H^{+}$).

29. Hong, L., Quinn, C. M. & Jia, Y. Evaluating the utility of the HTRF Transcreener ADP assay technology: a comparison with the standard HTRF assay technology. *Anal. Biochem.* **391,** 31–38 (2009).
30. Engelman, J. A. *et al.* ErbB-3 mediates phosphoinositide 3-kinase activity in gefitinib-sensitive non-small cell lung cancer cell lines. *Proc. Natl Acad. Sci. USA* **102,** 3788–3793 (2005).
31. Beard, C., Hochedlinger, K., Plath, K., Wutz, A. & Jaenisch, R. Efficient method to generate single-copy transgenic mice by site-specific integration in embryonic stem cells. *Genesis* **44,** 23–28 (2006).
32. Muller, G. W. Cyclic amides. *US patent* 5698579 (1997).

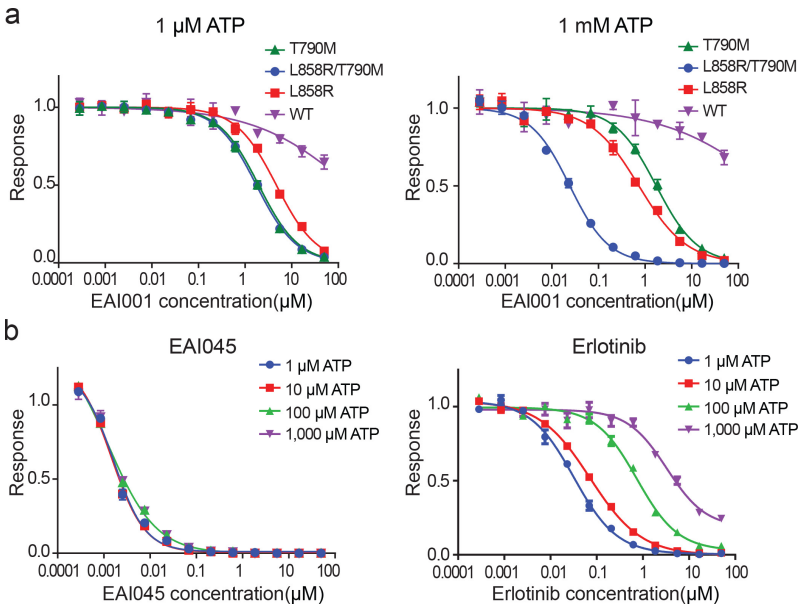

Extended Data Figure 1 | Inhibition of wild-type and mutant EGFR kinases by EAI001 and EAI045 in purified enzyme assays. a, Inhibition of wild-type and mutant EGFR kinases by EAI001. Activity of the indicated mutant EGFR kinase (residues 696–1022) was measured in the presence of increasing concentrations of EAI001. The HTRF assay was carried out using either 1 μM ATP (left) or 1 mM ATP (right). **b**, Inhibition of EGFR(L858R/T790M) by EAI045 (left) or erlotinib (right) at a range of ATP concentrations, as indicated. Assay was performed using an HTRF-based assay as described in the Methods. Error bars indicate s.d. ($n = 2$).

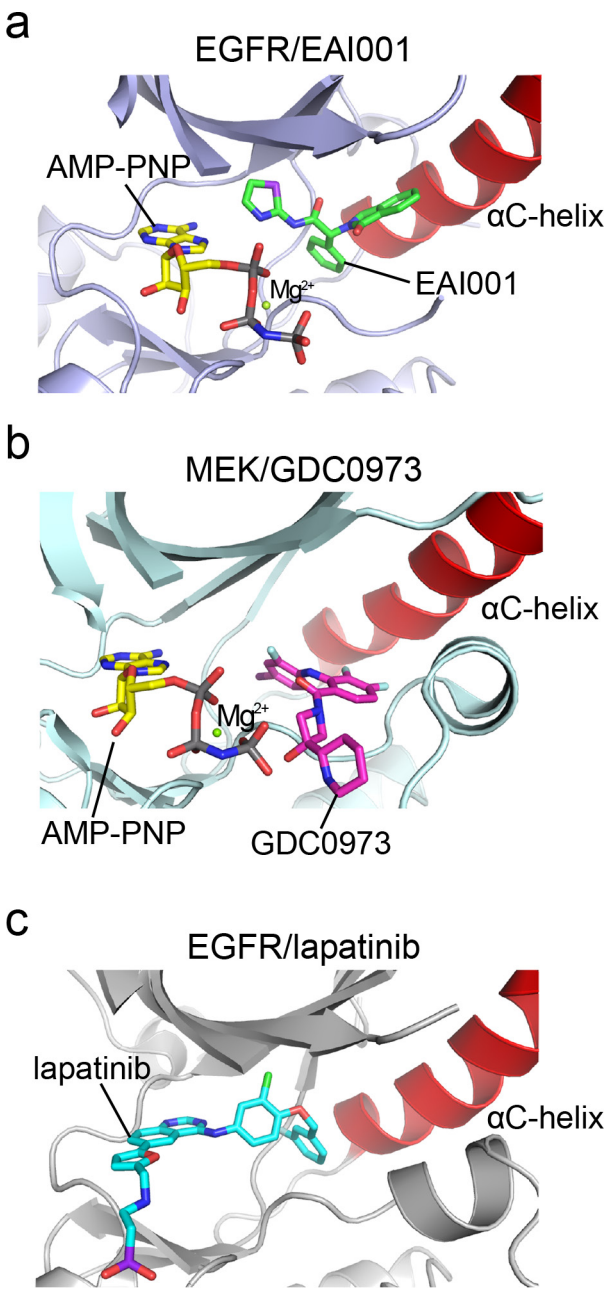

Extended Data Figure 2 | Comparison of the binding site of EGFR allosteric inhibitors with those of lapatinib and allosteric MEK inhibitors. a, Structure of EAI001 in complex with EGFR for comparison. **b**, Structure of MEK1 kinase bound to allosteric inhibitor GDC0973 (PDB, 4AN2). GDC0973 (also called XL518, cobimetinib) and other allosteric MEK inhibitors occupy a pocket created by displacement of the C-helix in the inactive conformation of the kinase. Most allosteric MEK inhibitors make hydrogen-bond interactions with the γ-phosphate group of ATP that are important for their potency. The allosteric EGFR inhibitors we describe here bind in a generally analogous location in EGFR, but lack any clear structural similarity to MEK inhibitors and do not contact the γ-phosphate group of ATP. **c**, The structure of lapatinib bound to EGFR (PDB, 1XKK). Both lapatinib and neratinib (see Fig. 1d) bind an inactive conformation of the kinase. Like gefitinib and erlotinib, both occupy the ATP site, but also extend into the allosteric pocket occupied by EAI001. Note that like neratinib, lapatinib places aromatic phenyl or pyridinyl groups in positions similar to those occupied by the aminothiazole and phenyl substituents of EAI001.

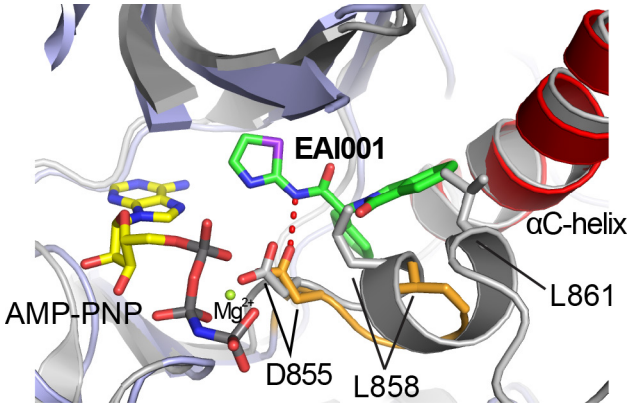

Extended Data Figure 3 | EAI001 binding is incompatible with the inactive conformation of wild-type EGFR. Superposition of the EAI001-bound EGFR structure reported here with the structure of wild-type EGFR kinase in the inactive conformation (grey, PDB, 2GS7). EAI001 (shown with carbon atoms in green) clashes with the side chains of leucines 858 and 861 in the wild-type EGFR structure. These leucine residues lie in a short helical segment at the N terminus of the activation loop. The L858R substitution disrupts this helix. We propose that this effect explains, in part, the selectivity of the allosteric inhibitor for the L858R/T790M mutant. Note that EAI001 was crystallized with the EGFR(T790M/V948R), as we were unable to obtain crystals with the L858R/T790M or L858R/T790M/V948R proteins. The compound induces unstructuring of the activation loop helix and repositions L858, which is in contact with the 1-oxoisoindolinyl group of the inhibitor. The location and conformation of the inhibitor is expected to be the same in the context of the L858R mutation, but the details of the interaction with this portion of the activation loop will necessarily differ due to the mutation.

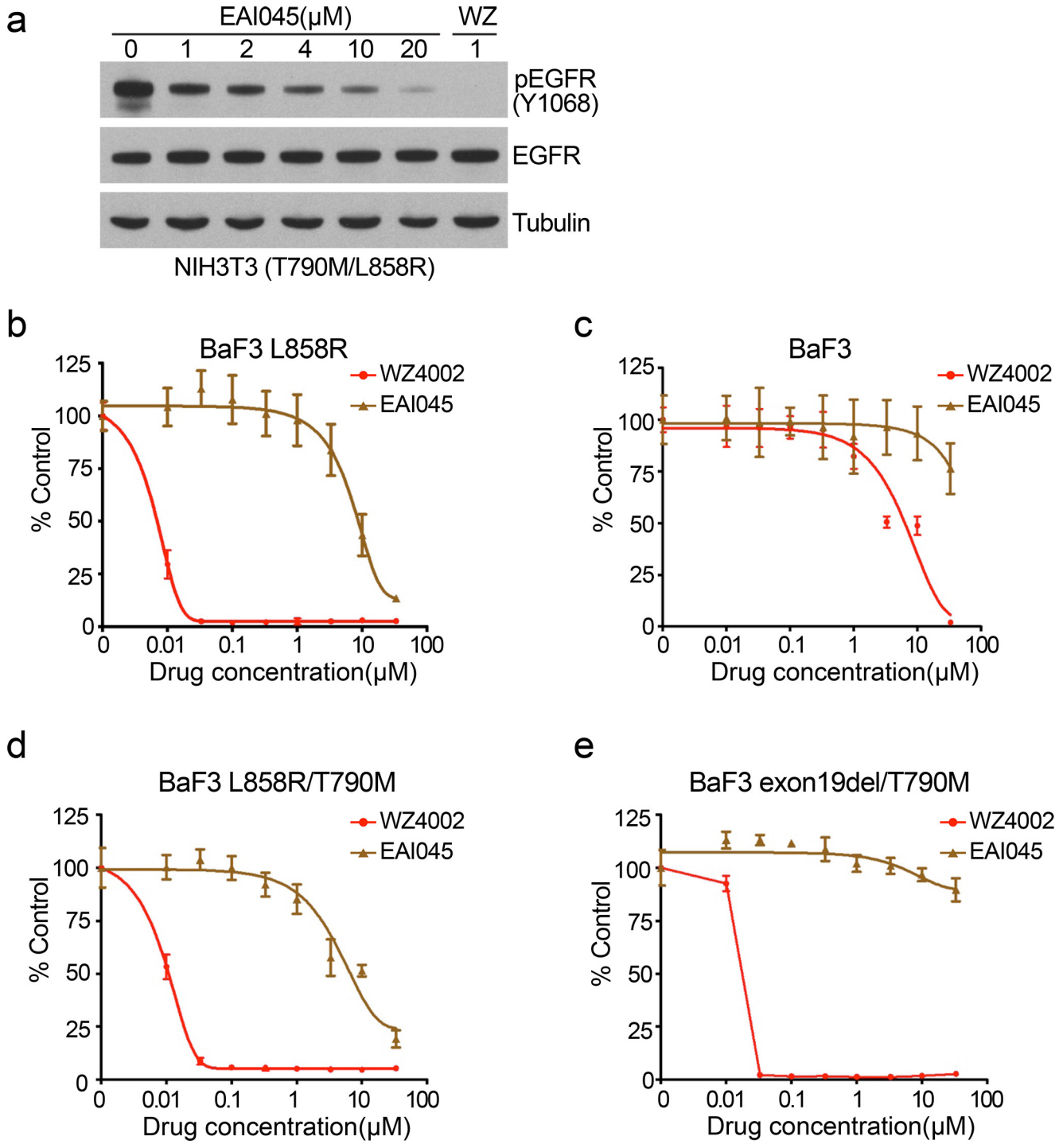

Extended Data Figure 4 | Cellular activity of EAI045. a, EAI045 inhibition of EGFR(L858R/T790M) in NIH-3T3 cells. Western blotting with the indicated concentrations of the allosteric inhibitor or with 1 μM WZ4002 as control (WZ) was carried out 6 h after compound addition. **b–e**, Profiling of EAI045 in Ba/F3 models bearing mutant EGFR or the parental Ba/F3 cell line, as indicted. Inhibition by WZ4002 is shown as a positive control. For gel source data, see Supplementary Fig. 1.

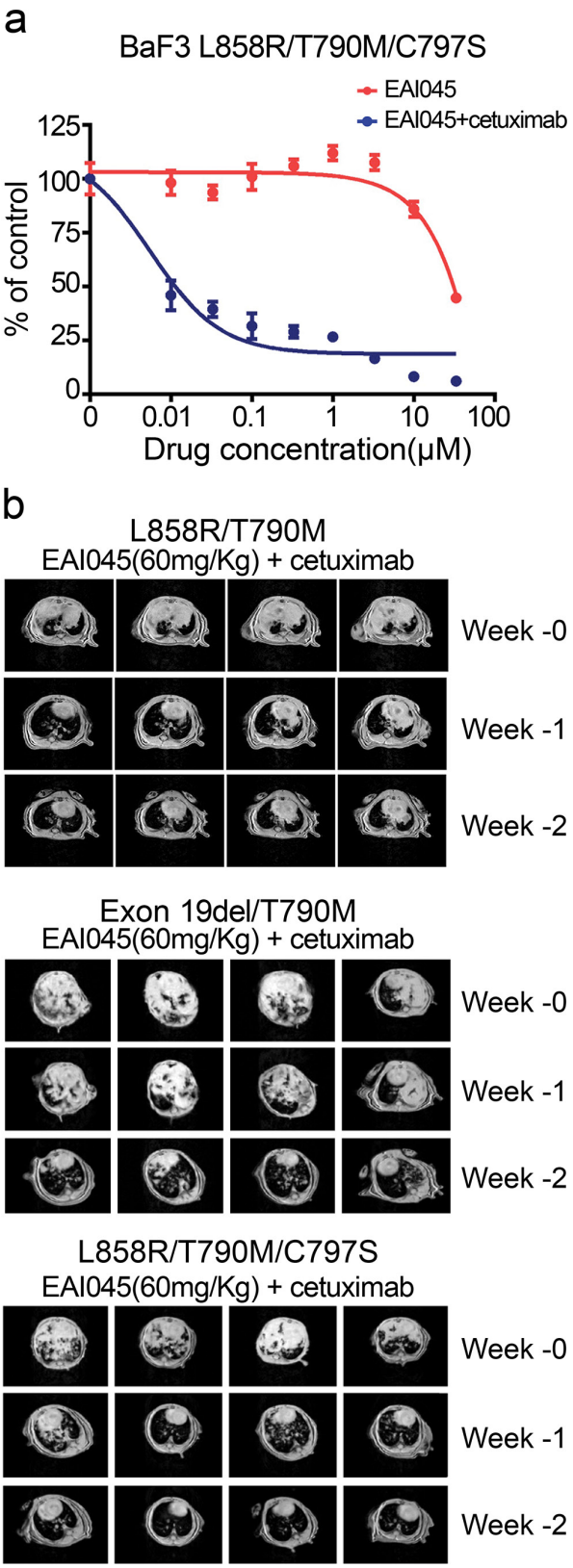

Extended Data Figure 5 | Cellular and *in vivo* efficacy of EAI045 in combination with cetuximab. a, Ba/F3 cells bearing EGFR(L858R/T790M/C797S) were treated with EAI045 alone or with EAI045 plus cetuximab and proliferation was measured using the MTS assay after 72 h. **b**, MRI imaging of cohorts L858R/T790M, exon19del/T790M, and L858R/T790M/C797S genetically engineered EGFR-mutant mice before treatment and 1 or 2 weeks after treatment with EAI045 and cetuximab. These cohorts of tumour bearing mice were used for short term efficacy and pharmacodynamic studies, and are distinct from those used for the tumour volume measurements shown in Fig. 3.

Extended Data Table 1 | The selectivity of EAI045 on a panel of kinases

Kinase	% inhibition	Kinase	% inhibition	Kinase	% inhibition	Kinase	% inhibition	Kinase	% inhibition	Kinase	% inhibition
ABL1	1	CK1-EPSILON	0	FMS	0	MAP4K5	13	PAK4	0	ROCK1	0
AKT1	0	CK1-GAMMA1	2	FRAP1	0	MAPK1	0	PAK5	0	ROCK2	0
AKT2	0	CK1-GAMMA2	0	FYN	0	MAPK3	0	PAK6	0	RON	0
AKT3	0	CK1-GAMMA3	6	GRK3	0	MAPKAPK2	0	PASK	1	ROS	1
ALK2	0	CK2	0	GRK5	0	MAPKAPK3	0	PDGFR-ALPHA	0	RSK1	0
ALK5	0	CLK1	0	GRK6	0	MARK1	0	PDGFR-BETA	4	RSK2	0
ALK6	0	CLK2	1	GRK7	0	MARK3	0	PDK1	0	RSK3	0
AMP-A1B1G1	1	CLK3	0	GSK-3-ALPHA	6	MARK4	0	PHK-GAMMA1	0	RSK4	0
AMP-A2B1G1	0	CLK4	0	GSK-3-BETA	0	MEK1	0	PHK-GAMMA2	0	SGK1	6
ARG	2	CRAF	0	HASPIN	1	MEK2	0	PI3K-ALPHA	0	SGK2	0
ARK5	0	CSK	0	HCK	0	MELK	0	PI3K-BETA	0	SGK3	0
AURORA-A	0	DAPK1	0	HIPK1	1	MER	8	PI3K-DELTA	0	SIK	0
AURORA-B	4	DAPK3	1	HIPK2	2	MET	0	PI3K-GAMMA	0	SLK	0
AURORA-C	0	DCAMKL2	0	HIPK3	0	MKNK1	0	PI4-K-BETA	9	SNF1LK2	0
AXL	4	DDR2	4	HIPK4	0	MNK2	3	PIM1	0	SPHK1	0
BLK	3	DYRK1A	0	IGF1R	4	MRCK-ALPHA	0	PIM2	2	SPHK2	0
BMX	1	DYRK1B	2	IKK-ALPHA	16	MRCK-BETA	0	PIM3	1	SRC	0
BRAF	0	DYRK3	2	IKK-BETA	0	MSK1	0	PKA	3	SRMS	0
BRK	0	DYRK4	1	IKK-EPSILON	0	MSK2	2	PKACB	0	SRPK1	0
BRSK1	0	EGFR	7	INSR	0	MSSK1	0	PKC-ALPHA	0	SRPK2	10
BRSK2	0	EPH-A1	0	IRAK1	4	MST1	0	PKC-EPSILON	14	STK16	0
BTK	0	EPH-A2	7	IRAK4	0	MST2	0	PKC-ETA	0	SYK	0
CAMK1A	0	EPH-A3	1	IRR	0	MST3	0	PKC-GAMMA	0	TAK1-TAB1	0
CAMK1D	0	EPH-A4	0	ITK	0	MST4	0	PKC-IOTA	0	TAOK2	0
CAMK2A	2	EPH-A5	4	JAK1	0	MUSK	0	PKC-THETA	0	TAOK3	0
CAMK2B	0	EPH-A8	0	JAK2	2	NDR1	2	PKC-ZETA	0	TBK1	3
CAMK2D	4	EPH-B1	0	JAK3	0	NDR2	0	PKN1	0	TEC	4
CAMK2G	9	EPH-B2	0	JNK1	0	NEK1	0	PKN2	1	TIE2	0
CAMK4	1	EPH-B3	0	JNK2	0	NEK2	2	PLK1	7	TNIK	0
CDK1	2	EPH-B4	0	JNK3	0	NEK3	0	PLK3	5	TNK1	0
CDK2-CYCLINA	1	ERB-B2	4	KDR	0	NEK6	0	PLK4	0	TNK2	2
CDK2-CYCLINE	0	ERB-B4	16	KIT	0	NEK7	0	PRAK	0	TRKA	0
CDK3-CYCLINE	0	FER	4	LATS2	2	NEK9	0	PRKD1	0	TRKB	3
CDK4-CYCLIND	0	FES	2	LCK	0	P38-ALPHA	0	PRKD2	2	TRKC	4
CDK5	0	FGFR1	5	LIMK1	0	P38-BETA	0	PRKD3	0	TSSK1	2
CDK5-P25	0	FGFR2	1	LOK	1	P38-DELTA	0	PRKG1	0	TSSK2	0
CDK6-CYCLIND3	2	FGFR3	1	LRRK2-G2019S	0	P38-GAMMA	2	PRKG2	8	TTK	0
CDK7	0	FGFR4	0	LTK	1	P70S6K1	0	PRKX	3	TXK	0
CDK9-CYCLINT1	6	FGR	0	LYNA	9	P70S6K2	0	PTK5	0	TYK2	0
CHEK1	0	FLT-1	8	LYNB	3	PAK1	0	PYK2	4	TYRO3	0
CHEK2	0	FLT-3	0	MAP4K2	0	PAK2	0	RET	0	YES	0
CK1	0	FLT-4	1	MAP4K4	2	PAK3	0	RIPK2	0	ZAP70	1

*Percent inhibition was measured in the presence of 1 μm EAI045. Experiment was performed once with duplicate samples.

Extended Data Table 2 | Selectivity of EAI045 against a panel of non-kinase targets

Assay Name	IC_{50} (μM)
Adenosine 2A receptor binding assay	>30
Adenosine 3 receptor binding assay	>30
Adrenergic Alpha 2C receptor assay	>30
Alpha1A adrenergic calcium flux assay (agonist mode)	>30
Alpha1A adrenergic calcium flux assay (antagonist mode)	>30
Beta 1 adrenergic receptor assay	>30
COX-1 assay	>30
CYP3A4 Induction Reporter Gene	>10
Dopamine D2 receptor assay	>30
Dopamine Transporter assay	>30
H1 receptor calcium assay (agonist mode)	>30
H1 receptor calcium assay (antagonist mode)	>30
Histamine H1 receptor assay	>30
Melanocortin MC3 receptor binding assay	>30
Monoamine Oxidase A assay	>30
Muscarinic M1 receptor assay	>30
Muscarinic M2 calcium flux assay with ATP priming (agonist mode)	>30
Nicotinic (CNS) Receptor binding (human IMR32 cells)	>30
Norepinephrine Transporter assay	>30
PPARgamma Receptor agonist assay	>30
PPARgamma Receptor antagonist assay	>30
PXR Receptor agonist assay	16
PXR Receptor antagonist assay	>3
Phosphodiesterase 3 assay (human platelets)	>30
Phosphodiesterase 4D assay	>30
Pregnane X Receptor (PXR; SXR) binding assay	7
Progesterone Receptor agonist assay	>30
Progesterone Receptor antagonist assay	>30
Serotonin 5HT2A calcium flux assay (agonist mode)	>30
Serotonin 5HT2A calcium flux assay (antagonist mode)	>30

Extended Data Table 3 | Crystallographic data collection and refinement statistics

Crystal name	EGFR T790M/V948R EAI001
Data collection	
Space group	C2
Cell dimensions	
a, b, c (Å)	155.1, 72.5, 76.0
α, β, γ (°)	90, 113.2, 90
Resolution (Å)	42.24 - 2.31 (2.39)*
R_{merge}	0.11 (0.51)
I/σ	10.4 (1.9)
Completeness (%)	97.8 (94.0)
Redundancy	3.4 (2.9)
Refinement	
Resolution (Å)	42.24 - 2.31
No. Reflections	33377
R_{work}/ R_{free}	0.174/0.206
No. Atoms	
Protein	4826
Ligand/ion (AMPPNP/EAI001/Mg^{2+})	62/25/2
Water	398
B-factors	
Protein	33.70
Ligand/ion (AMPPNP/EAI001/Mg^{2+})	25.90
Water	36.60
R.m.s deviations	
Bond lengths (Å)	0.008
Bond angles (°)	1.136

Diffraction data were recorded from a single crystal.
*Values in parentheses are for highest resolution shell.

Extended Data Table 4 | Cellular activity of EAI045 in lung cancer cell lines

	EAI045 EC_{50} (μM)	
Cell line (EGFR)	Target modulation*	Proliferation†
H1975 (L858R/T790M)	0.002 (4)	>10 (2)
H3255 (L858R)	0.163 (4)	>10 (2)
HaCaT (WT)	>10 (2)	>10 (1)

*ELISA-based assay for phosphorylation of EGFR Y1173; the number of times each experiment was repeated is given in parentheses.
†The number of times each experiment was repeated is given in parentheses.